

Two cosmological models for clusters of galaxies

Ivan Suhhonenko and Mirt Gramann

Tartu Observatory, Tõravere EE-2444, Estonia

3 January 2018

ABSTRACT

We investigate the properties of clusters of galaxies in two cosmological models using N-body simulations and the Press-Schechter (PS) theory. In the first model, the initial power spectrum of density fluctuations is in the form $P(k) \propto k^{-2}$ at wavelengths $\lambda < 120h^{-1}$ Mpc. In the second model, the initial linear power spectrum of density fluctuations contains a feature (bump) at wavelengths $\lambda \sim 30 - 60h^{-1}$ Mpc which correspond to the scale of superclusters of galaxies. We examine the mass function, peculiar velocities, the power spectrum and the correlation function of clusters in both models for different values of the density parameter Ω_0 and σ_8 (the rms fluctuation on the $8h^{-1}$ Mpc scale). The results are compared with observations. We find that in many aspects the power spectrum of density fluctuations in the model (2) fits the observed data better than the simple power law model (1). In the first model, the mass function and peculiar velocities of clusters are consistent with observations only if $\Omega_0 < 0.6$. In the second model, the permitted region in the (Ω_0, σ_8) plane is larger. In this model, the power spectrum of clusters is in good agreement with the observed power spectrum of the APM clusters. This model predicts that there is a bump in the correlation function of clusters at separations $r \sim 20 - 35h^{-1}$ Mpc. In the future, accurate measurements of the cluster correlation function at these distances can serve as a discriminating test for this model.

We examine the linear theory predictions for the peculiar velocities of peaks in the Gaussian field and compare these to the peculiar velocities of clusters in N-body simulations. We determine the clusters as the maxima of the density field smoothed on the scale $R \sim 1.5h^{-1}$ Mpc and define their peculiar velocities using the same smoothing scale as for the density field. The numerical results show that in this case the rms peculiar velocities of clusters increase with cluster richness. The rms peculiar velocity of small clusters is similar to the linear theory expectations, while the rms peculiar velocity of rich clusters is higher than that predicted in the linear theory ($\sim 18\%$ for clusters with a mean intercluster separation $d_{cl} = 30h^{-1}$ Mpc).

Key words: cosmology: theory – large-scale structure of Universe, cosmology: theory – dark matter, galaxies: clusters

1 INTRODUCTION

The formation of structure in our Universe is one of the most fascinating problems in cosmology. Usually we believe that galaxies and clusters of galaxies have developed by gravitational instability out of small inhomogeneities of the early Universe. The initial field of density fluctuations $\delta(\mathbf{x}, t)$ can be decomposed into its Fourier components $\delta_{\mathbf{k}}(t)$ and expressed in terms of the power spectrum $P(k) = \langle |\delta_{\mathbf{k}}|^2 \rangle$.

Figure 1 shows the observed power spectra derived from the distribution of galaxies in the APM, Stromlo-APM and SSRS2+CfA2 surveys (Baugh & Efstathiou 1993; Tadros & Efstathiou 1996; Costa et al. 1994). The power spectrum of the galaxy distribution in the Stromlo-APM redshift sur-

vey peaks at the wavenumber $k = 0.052h$ Mpc $^{-1}$ (or at the wavelength $\lambda = 120h^{-1}$ Mpc). A similar peak in the one-dimensional power spectrum of a deep pencil-beam survey was detected by Broadhurst et al. (1990) and in the two-dimensional power spectrum of the Las Campanas redshift survey by Landy et al. (1996). Available data, however, are insufficient to say whether the peak in the Stromlo-APM survey reflects a real feature in the galaxy distribution. It is likely that the decline in the power spectrum at wavenumbers $k \leq 0.052h$ Mpc $^{-1}$ is partly due to the effects of the uncertainty in the mean number density of optical galaxies (see Tadros & Efstathiou 1996 for a discussion of this effect). However, independent evidence for the presence of a

arXiv:astro-ph/9806177v2 11 Dec 1998

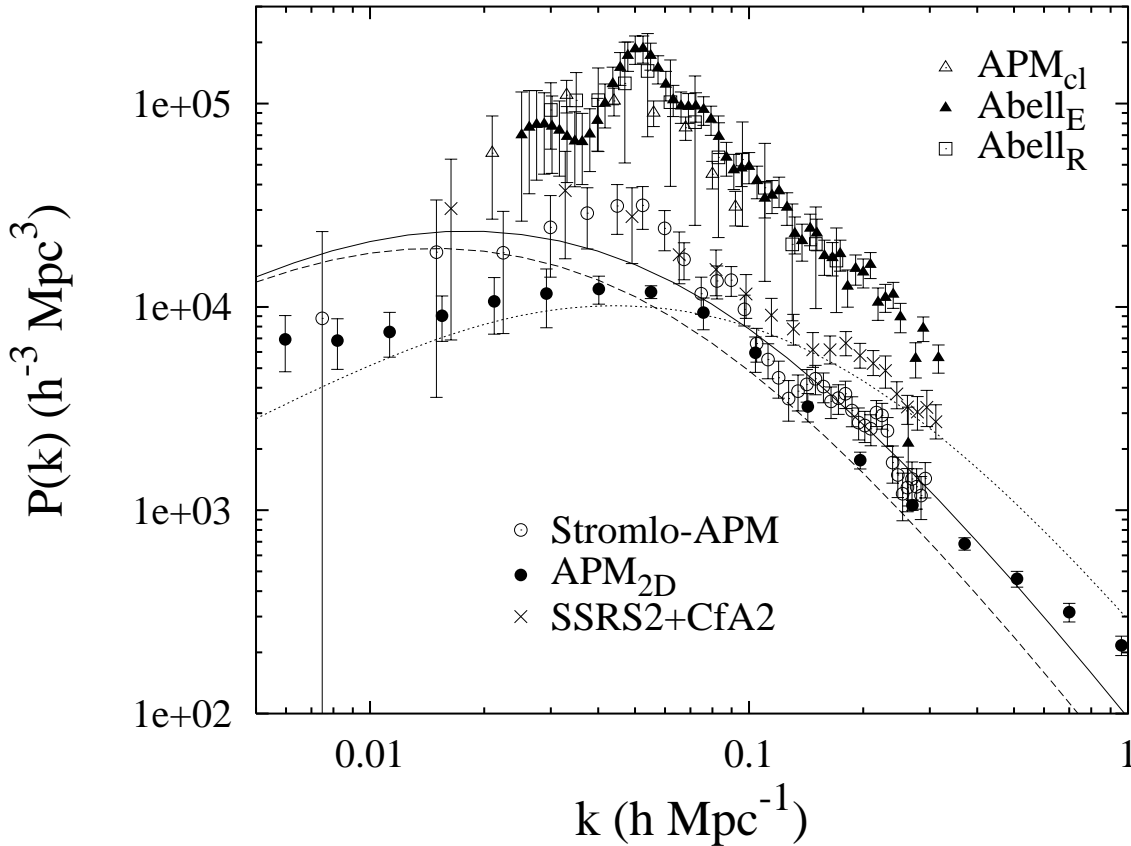


Figure 1. The power spectrum of the distribution of galaxies and clusters of galaxies. Filled circles, open circles and crosses show the power spectrum of the galaxy distribution in the APM, Stromlo-APM and SSRS2+CfA2 surveys, respectively. Filled triangles and open squares show the power spectrum of the distribution of Abell clusters as determined by Einasto et al. (1997a) and Retzlaff et al. (1998), respectively. Open triangles represent the power spectrum of APM clusters. For comparison, we show the linear power spectrum of density fluctuations in the flat CDM models with $\Omega_0 = 0.3$ and $h = 0.7$ (solid line) and $h = 0.6$ (dashed line). The dotted line shows the power spectrum in the CDM model with $\Omega = 1$ and $h = 0.5$. The CDM models are COBE-normalized.

preferred scale in the Universe at about $120h^{-1}$ Mpc comes from an analysis of the distribution of galaxy clusters. Figure 1 shows the power spectrum of the distribution of the Abell-ACO clusters as determined by Einasto et al. (1997a) and Retzlaff et al. (1998), and the power spectrum of the APM clusters as measured by Tadros, Efstathiou & Dalton (1998). The power spectrum of the distribution of the Abell-ACO clusters has a well-defined peak at the same wavenumber, $k_0 = 0.052h$ Mpc $^{-1}$, as the power spectrum of galaxies in the Stromlo-APM survey. For wavenumbers $k > k_0$, the shape of the clusters' power spectrum is similar to the shape of the power spectrum for galaxies in the Stromlo-APM survey. This comparison suggests that the peak observed in the power spectrum of the Stromlo-APM redshift survey is a real feature in the distribution of galaxies (see Gramann (1998) for a more detailed discussion of the observed power spectra in different galaxy surveys).

Cosmological models based on collisionless dark matter (e.g. cold dark matter (CDM)) and adiabatic fluctuations, when combined with power-law initial power spectra, predict smooth power spectra of density fluctuations at $z \sim 10^3$. Figure 1 shows the power spectra of density fluctuations

predicted in the flat CDM models with the density parameter $\Omega_0 = 0.3$ and the normalized Hubble constant $h = 0.6$ and $h = 0.7$. For comparison, we show in Figure 1 the power spectrum predicted in the CDM model with $\Omega = 1$ and $h = 0.5$. We have used the transfer function derived by Bardeen et al. (1986) and Sugiyama (1995), and the COBE normalization derived by Bunn and White (1997). The observed power spectra of galaxies and clusters of galaxies are not consistent with CDM-type models (see also e.g. Peacock 1997; Einasto et al. 1997a; Tadros, Efstathiou & Dalton 1998). The baryonic acoustic oscillations in adiabatic models may explain the observed excess only if currently favored determinations of cosmological parameters are in substantial error (e.g. the density parameter $\Omega_0 < 0.2h$) (Eisenstein et al. 1998). One possible explanation for the presence of a peak in the power spectrum is an inflationary scenario with a scalar field whose potential has a localized feature around some value of the field (Starobinsky 1992; Lesgourgues, Polarski & Starobinsky 1998).

In this paper we study the properties and spatial distribution of galaxy clusters in two cosmological models which start from the observed power spectra of the distribution of

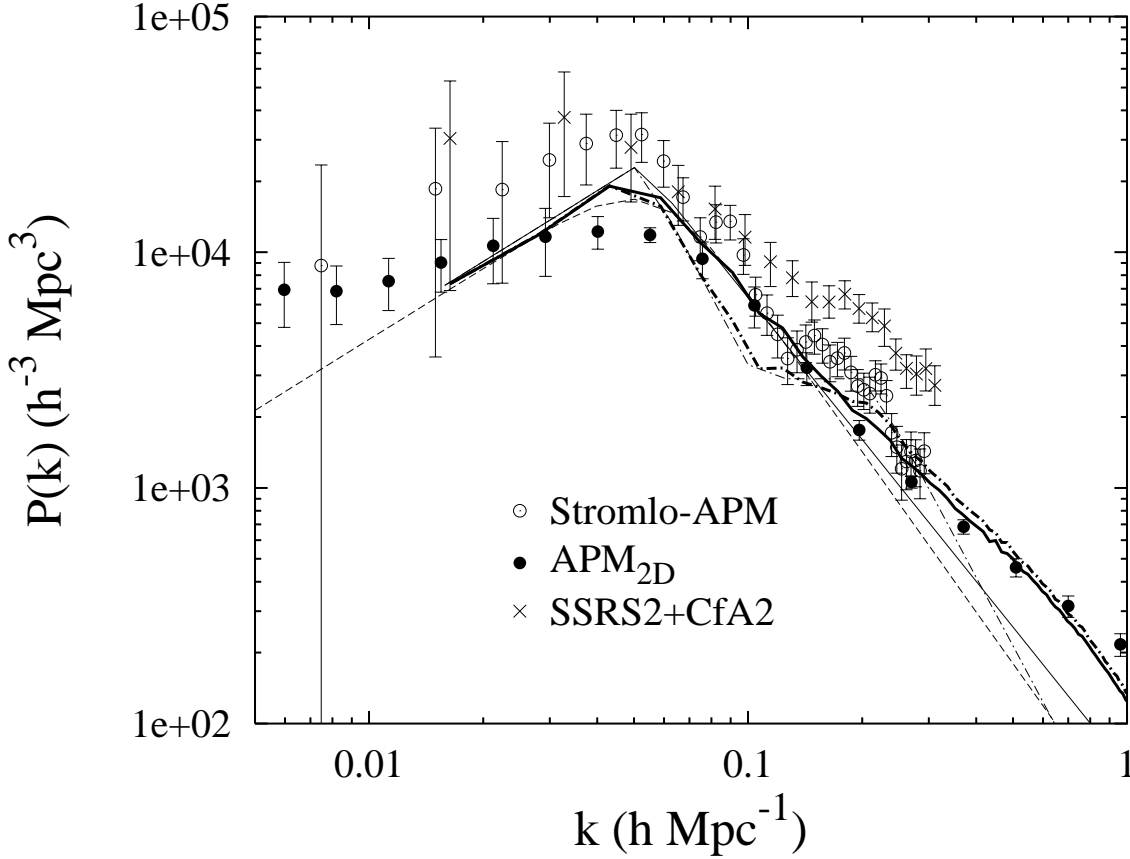


Figure 2. The linear and non-linear power spectra of density fluctuations in the model (1) (solid lines) and in the model (2) (dot-dashed lines). The heavy curves show the results of the N-body simulations and the light curves the corresponding linear power spectra. The dashed line shows the linear power spectrum derived by Peacock (1997). Filled circles, open circles and crosses show the power spectrum of the galaxy distribution in the APM, Stromlo-APM and SSRS2+CfA2 surveys, respectively.

galaxies. In the first model we assume that the initial linear power spectrum of density fluctuations in the universe at $z \sim 10^3$ is of the form

$$P(k) = \begin{cases} P(k_0)(k/k_0), & \text{if } k < k_0; \\ P(k_0)(k/k_0)^{-2}, & \text{if } k > k_0, \end{cases} \quad (1)$$

where $k_0 = 0.052h \text{ Mpc}^{-1}$ and $P(k_0) = 3.71 \times 10^4 \sigma_8^2 h^{-3} \text{ Mpc}^3$. The σ_8 is the rms mass fluctuation on the $8h^{-1} \text{ Mpc}$ scale. Gramann (1998) used the function (1) to recover the power spectrum in the Stromlo-APM redshift survey. In the second model we assume that the linear power spectrum contains a primordial feature at wavenumbers $k \sim 0.1 - 0.2h \text{ Mpc}^{-1}$ ($\lambda \sim 30 - 60h^{-1} \text{ Mpc}$) which correspond to the scale of superclusters, and

$$P(k) = \begin{cases} P(k_0)(k/k_0), & \text{if } k < k_0; \\ P(k_0)(k/k_0)^{-3}, & \text{if } k_0 < k < k_1; \\ P(k_1), & \text{if } k_1 < k < k_2; \\ P(k_1)(k/k_0)^{-3}, & \text{if } k > k_2, \end{cases} \quad (2)$$

where $k_0 = 0.052h \text{ Mpc}^{-1}$, $k_1 = 0.1h \text{ Mpc}^{-1}$, $k_2 = 0.2h \text{ Mpc}^{-1}$, $P(k_0) = 3.34 \times 10^4 \sigma_8^2 h^{-3} \text{ Mpc}^3$ and $P(k_1) = 4.07 \times 10^3 \sigma_8^2 h^{-3} \text{ Mpc}^3$. We assume also that the initial density fluctuation field in the Universe is a Gaussian field. In

this case the power spectrum provides a complete statistical description of the field.

Figure 2 demonstrates the linear and nonlinear power spectra of density fluctuations in the model (1) for $\sigma_8 = 0.8$ and in the model (2) for $\sigma_8 = 0.84$. To examine the nonlinear evolution of density fluctuations we have used N-body simulations. The parameters of the simulations are given in Section 3. We see that at wavenumbers $k > 0.2h^{-1} \text{ Mpc}$, the nonlinear power spectra in models (1) and (2) are very similar. Figure 2 shows also the power spectra of the galaxy clustering in the APM, Stromlo-APM and SSRS2+CfA2 surveys (Baugh & Efstathiou 1993; Tadros & Efstathiou 1996; Costa et al. 1994). The spatial distribution of galaxies in the models (1) and (2) depends on the relation between galaxies and matter density, and further study is needed to study galaxies in these models. Figure 2 demonstrates that if we assume a linear bias between galaxies and density, the initial power spectra given by equations (1) and (2) are in good agreement with the observed power spectra of galaxies. For comparison, we show in Figure 2 the linear power spectrum derived from the observed galaxy power spectra by Peacock (1997) (we have used his eq. [34] with parameters given in eq. [35]). The initial power spectrum derived by Peacock (1997) is similar to the function (1).

In this paper we examine the evolution of the mass function, peculiar velocities, the power spectrum and the correlation function of galaxy clusters in models (1) and (2) for different values of the density parameter Ω_0 and σ_8 . To study the mass function of clusters of galaxies, we use the Press-Schechter (1974) formalism. To investigate peculiar velocities and the spatial distribution of galaxy clusters, we use N-body simulations.

In the simulations we use the equations of motion for the model with $\Omega = 1$. According to the equations of motion, expressed in terms of the linear growing mode, the evolution of a pressureless fluid in an expanding universe is almost independent of the density parameter Ω_0 and of the cosmological constant Λ (e.g. Gramann 1993; Nusser & Colberg 1998). Nusser & Colberg (1998) used high resolution N-body simulations to investigate the effect of changing the cosmological background on the evolution of fluctuations and demonstrated that once the initial density fluctuation field is evolved to a given amplitude (e.g. $\sigma_8 \sim 0.7$) and smoothed on scales $R \geq 1h^{-1}$ Mpc, it is almost insensitive to the cosmological background. The smoothed nonlinear velocity field scales with the linear velocity growth factor, $f(\Omega_0) \approx \Omega_0^{0.6}$, just as it does in the linear theory. Therefore, if clusters represent the maxima of the density field which is smoothed on scales $R \sim 1 - 2h^{-1}$ Mpc, their spatial distribution in real space is not sensitive to Ω_0 and Λ .

Observations provide the distribution of clusters in the redshift space, which is distorted due to peculiar velocities of clusters. In order to study peculiar velocities of galaxy clusters and their distribution in the redshift space in the models with different Ω_0 , we determine the velocities of clusters in the simulations with $\Omega = 1$ and assume that peculiar velocities of galaxy clusters, as the whole velocity field, are proportional to the growth factor $f(\Omega_0)$. The linear velocity growth factor depends very weakly on the cosmological constant (e.g. Lahav et al. 1991) and in this paper we neglect this dependence.

This paper is organized as follows. In Section 2 we study the mass function of clusters of galaxies in our models and compare the results with observations. In Section 3 we examine peculiar velocities of galaxy clusters. In Section 4 we investigate the redshift-space power spectrum of clusters and in Section 5 we study the correlation function of clusters. Section 6 summarizes the main results.

A Hubble constant of $H_0 = 100h$ km s $^{-1}$ Mpc $^{-1}$ is used throughout this paper.

2 THE MASS FUNCTION OF CLUSTERS OF GALAXIES

To investigate the mass function of clusters we use the Press-Schechter (1974, PS) approximation. The PS mass function has been compared with N-body simulations (Efstathiou et al. 1988; White, Efstathiou & Frenk 1993; Lacey & Cole 1994; Eke, Cole & Frenk 1996; Borgani et al. 1997a) and has been shown to provide an accurate description of the abundance of virialized halos of cluster size. In the PS approximation the number density of clusters with the mass

between M and $M + dM$ is given by

$$n(M)dM = -\sqrt{\frac{2}{\pi}} \frac{\rho_b}{M} \frac{\delta_t}{\sigma^2(M)} \frac{d\sigma(M)}{dM} \exp\left[-\frac{\delta_t^2}{2\sigma^2(M)}\right] dM. \quad (3)$$

Here ρ_b is the mean background density and δ_t is the linear theory overdensity for a uniform spherical fluctuation which is now collapsing; $\delta_t = 1.686$ for $\Omega = 1$, with a weak dependence on Ω_0 for flat and open models (e.g. Eke et al. 1996). The function $\sigma(M)$ is the rms linear density fluctuation at the mass scale M . We will use the top-hat window function. For the top-hat window, the mass M is related to the window radius R as $M = 4\pi\rho_b R^3/3$. In this case, the number density of clusters of mass larger than M can be expressed as

$$n_{cl>(> M) = \int_M^\infty n(M')dM' = -\frac{3}{(2\pi)^{3/2}} \int_R^\infty \frac{\delta_t}{\sigma^2(r)} \frac{d\sigma(r)}{dr} \exp\left[-\frac{\delta_t^2}{2\sigma^2(r)}\right] \frac{dr}{r^3}. \quad (4)$$

Figure 3 shows the cluster mass function for the power spectra (1) and (2). We investigated the cluster masses within a $1.5h^{-1}$ Mpc radius sphere around the cluster center. This mass $M_{1.5}$, is related to the window radius R as

$$R = 8.43\Omega_0^{\frac{0.2\alpha}{3-\alpha}} \left[\frac{M_{1.5}}{6.99 \times 10^{14}\Omega_0 h^{-1}M_\odot} \right]^{\frac{1}{3-\alpha}} (h^{-1}\text{Mpc}). \quad (5)$$

Here the parameter α describes the cluster mass profile, $M(r) \sim r^\alpha$, at radii $r \sim 1.5h^{-1}$ Mpc. Numerical simulations and observations of clusters indicate that the parameter $\alpha \approx 0.6 - 0.7$ for most of clusters (Navarro, Frenk & White 1995; Carlberg, Yee & Ellingson 1997). In this paper we use a value $\alpha = 0.65$.

The number density of massive clusters is a sensitive function of Ω_0 and σ_8 . Figure 3a shows the mass function for the open models with $\Omega_0 = 0.3$, $\sigma_8 = 0.8$ and $\sigma_8 = 1.0$. In Figure 3b we present the mass function for the open models with $\Omega_0 = 0.4$, $\sigma_8 = 0.7$ and $\sigma_8 = 0.9$. The cluster abundances in models (1) and (2), when compared at the same values of Ω_0 and σ_8 , are very similar for smaller cluster masses, $M_{1.5} \leq 4 \times 10^{14}h^{-1}M_\odot$. For larger masses the mass function in the model (2) is steeper than in the model (1). We investigated also the cluster abundances for the flat models with slightly larger values of δ_t derived by Eke et al. (1996), and found that for a given Ω_0 and $M_{1.5}$, the cluster abundance for the flat model is $\sim 10\%$ smaller than for the open model.

Figure 3 shows also the mass function of clusters of galaxies derived by Bahcall and Cen (1993, BC) and by Girardi et al. (1998, G98). BC used both optical and X-ray observed properties of clusters to determine the mass function of clusters. The function was extended towards the faint end using small groups of galaxies. G98 determined the mass function of clusters by using virial mass estimates for 152 nearby Abell-ACO clusters including the new ENACS data (Katgert et al. 1998). The mass function derived by G98 is somewhat larger than the mass function derived by BC, the difference being larger at larger masses (see Figure 3). We find that the models with $\Omega_0 = 0.3$, $\sigma_8 = 0.8$ and $\Omega_0 = 0.4$, $\sigma_8 = 0.7$ provide good match to the mass function derived by

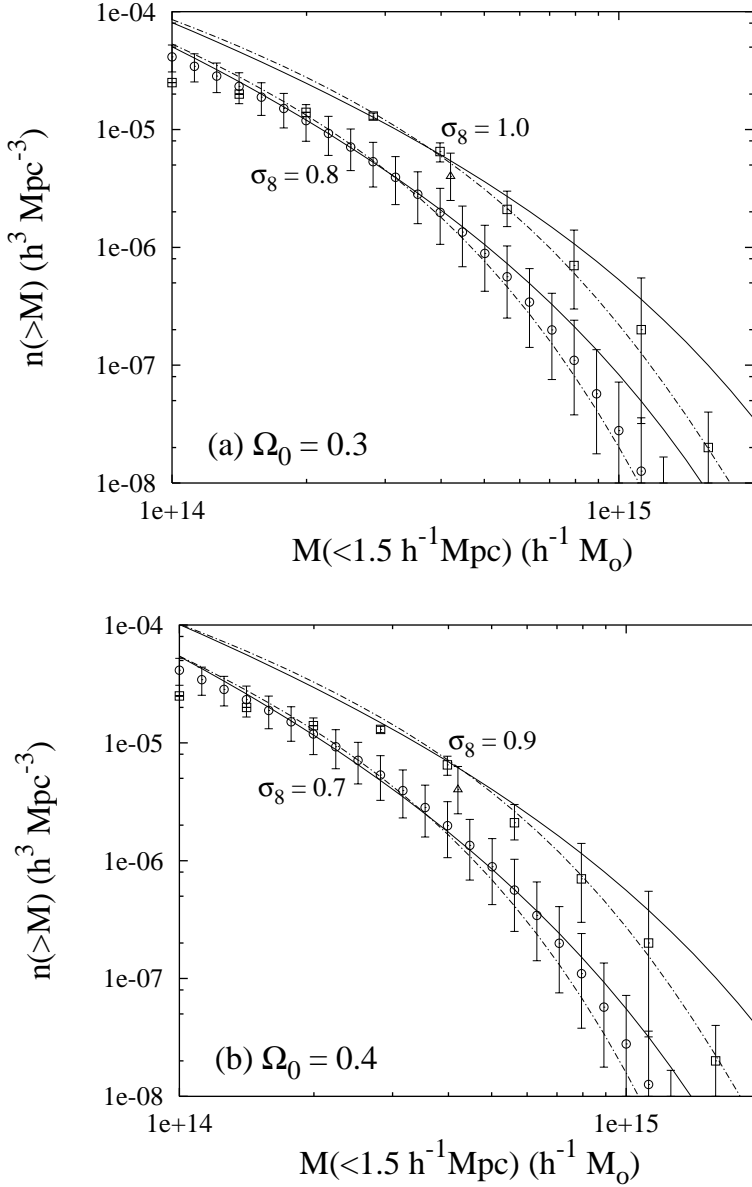


Figure 3. The cluster mass function in the model (1) (solid lines) and in the model (2) (dot-dashed lines). (a) The density parameter $\Omega_0 = 0.3$. The mass function is shown for $\sigma_8 = 0.8$ and for $\sigma_8 = 1.0$. (b) The density parameter $\Omega_0 = 0.4$. The mass function is shown for $\sigma_8 = 0.7$ and for $\sigma_8 = 0.9$. Open circles and squares show the mass function of galaxy clusters derived by Bahcall and Cen (1993) and by Girardi et al. (1998), respectively. The open triangle describes the result obtained by White, Efstathiou & Frenk (1993).

BC, whereas models with $\Omega_0 = 0.3$, $\sigma_8 = 1.0$ and $\Omega_0 = 0.4$, $\sigma_8 = 0.9$ are in good agreement with the data derived by G98.

Let us consider the amplitude of the mass function of galaxy clusters at $M_{1.5} = 4 \times 10^{14} h^{-1} M_\odot$. For this mass, the cluster abundances derived by BC and G98 are $n(> M) = (2.0 \pm 1.1) \times 10^{-6} h^3 \text{ Mpc}^{-3}$ and $n(> M) = (6.3 \pm 1.2) 10^{-6} h^3 \text{ Mpc}^{-3}$, respectively. By analysing X-ray properties of clusters, White, Efstathiou & Frenk (1993) found that the number density of clusters with mass $M_{1.5} \approx 4.2 \times 10^{14} h^{-1} M_\odot$ is $n(> M) = 4 \times 10^{-6} h^3 \text{ Mpc}^{-3}$. Figure 4 shows the limits for

$\sigma_8 \Omega_0^{0.6}$, assuming that the mass function of galaxy clusters at $M_{1.5} = 4 \times 10^{14} h^{-1} M_\odot$ is in the range $(2 - 6.5) \times 10^{-6} h^3 \text{ Mpc}^{-3}$. These limits are similar in both our models. For $\Omega_0 = 0.3$ and $\Omega_0 = 0.4$, we find that $\sigma_8 = 0.90 \pm 0.12$ and $\sigma_8 = 0.80 \pm 0.09$, respectively. For $\Omega = 1$, $\sigma_8 = 0.56 \pm 0.05$. These limits for σ_8 are very similar to the limits derived by Eke et al. (1996) for the CDM models by analyzing X-ray temperatures of clusters.

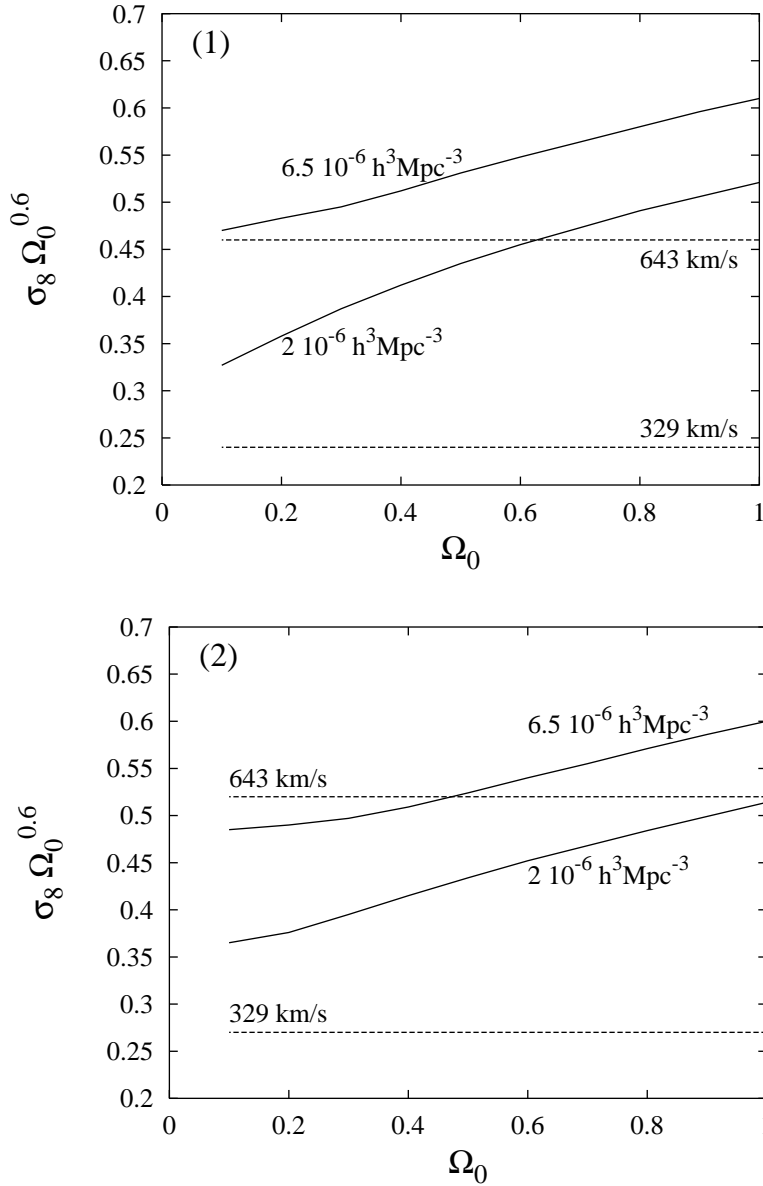


Figure 4. The limits for $\sigma_8 \Omega_0^{0.6}$ in the model (1) (upper panel) and in the model (2) (lower panel). Solid lines show the constraints obtained by studying the mass function of clusters and dashed lines show the constraints obtained by analyzing the peculiar velocities of clusters.

3 PECULIAR VELOCITIES OF CLUSTERS OF GALAXIES

To investigate peculiar velocities of galaxy clusters and their spatial distribution we used N-body simulations. The simulations examined in this paper were created using the particle-mesh code described by Gramann (1988). We investigated the evolution of 256^3 particles on a 256^3 grid, the comoving box size was $L = 384h^{-1}$ Mpc. Clusters were determined in the simulations at the moment when $\sigma_8 = 0.8$ and $\sigma_8 = 0.84$ in the models (1) and (2), respectively.

Clusters were selected in the simulations as maxima of

the density field that was determined on a 256^3 grid using the CIC-scheme. To determine peculiar velocities of clusters, we determined the peculiar velocity field on a 256^3 grid using the CIC-scheme and found the peculiar velocities at the grid points where the clusters had been identified. The clusters were then ranked according to their density and we selected $N_{cl} = (L/d_{cl})^3$ highest ranked clusters to produce cluster catalogs with a mean intercluster separation $d_{cl} = 10 - 100h^{-1}$ Mpc. For comparison, the number density of the observed APM clusters and Abell clusters is $n_{cl} \sim 3.4 \times 10^{-5} h^3 \text{Mpc}^{-3}$ ($d_{cl} \sim 31h^{-1}$ Mpc) and

$n_{cl} \sim 2.5 \times 10^{-5} h^3 \text{ Mpc}^{-3}$ ($d_{cl} \sim 34h^{-1} \text{ Mpc}$), respectively (Dalton et al. 1994, Einasto et al. 1997b, Retzlaff et al. 1998).

It is difficult to follow the evolution of rich clusters by using N-body simulations, as it requires simulations with a very large dynamical range to identify correctly a sufficient number of clusters. The grid size in our N-body simulations is $R_g = 1.5h^{-1} \text{ Mpc}$ and the cluster centers in the simulations are at least $3h^{-1} \text{ Mpc}$ apart. This could cause clusters to merge prematurely, and to have some effect on their properties. However, in order to increase the resolution of the simulations we must increase the number of test particles and grid points, or have to follow the evolution of clusters in a smaller box. While the first possibility is technically difficult, in the latter case the number of rich clusters becomes too small to get statistically reliable results. Taking into account the requirements on the number of clusters and on the resolution together with the fact of fixed computer resources we decided to use a box size $L = 384h^{-1} \text{ Mpc}$ and a grid size $R_g = 1.5h^{-1} \text{ Mpc}$.

To determine the rms peculiar velocities of clusters, we used the equation

$$v_{cl}^2 = v_s^2 + v_L^2 = \frac{1}{N_{cl}} \sum_{i=1}^{N_{cl}} v_i^2 + v_L^2, \quad (6)$$

where the parameter v_s describes the dispersion of the cluster velocities, v_i , derived from the simulation and the parameter v_L is given by

$$v_L^2 = f^2(\Omega_0) H_0^2 \left[\frac{1}{2\pi^2} \int_0^\infty P(k) dk - \frac{1}{L^3} \sum_{\mathbf{k}_s} \frac{P_s(\mathbf{k})}{k^2} \right]. \quad (7)$$

The last term in this expression is a discrete sum over the linear modes in the simulation, \mathbf{k}_s , with the power per mode, $P_s(\mathbf{k})$, as actually used in the simulation. We found that for clusters with a mean separation $d_{cl} \geq 30h^{-1} \text{ Mpc}$, $v_L^2/v_s^2 \sim 4.9\%$ and $v_L^2/v_s^2 \sim 3.7\%$, in models (1) and (2), respectively.

Figure 5 shows the rms peculiar velocities of clusters, v_{cl} , in models (1) and (2), for the same values of Ω_0 and σ_8 as in Figure 3. The rms peculiar velocities of clusters in the model (2) are $\sim 12\%$ smaller than in the model (1), when compared at the same values of Ω_0 and σ_8 . Figure 5 shows the rms peculiar velocities for different values of the mean cluster separation, d_{cl} . We see that the rms peculiar velocities of clusters increase with cluster richness. In both models studied, the rms peculiar velocity of very massive clusters with an intercluster separation $d_{cl} = 80h^{-1} \text{ Mpc}$ is $\sim 25\%$ higher than the rms velocity of the clusters with a separation $d_{cl} = 20h^{-1} \text{ Mpc}$.

We note that this effect is sensitive to the algorithms used to define clusters and to determine their peculiar velocities. When we determined the clusters using the standard friends-of-friends algorithm (FOF) and defined the peculiar velocity of each cluster to be the mean peculiar velocity of all the particles within the cluster, we found that the rms peculiar velocities of clusters decrease with cluster richness. This is because with the FOF algorithm we identify almost the same objects as with the algorithm used throughout this paper, but the sizes of objects are different — poor clusters are smaller and rich clusters are larger. The peculiar velocity of the cluster, as the mass of the cluster, depends on the size of the cluster. The larger the smoothing region, the smaller the velocity.

In this paper we have determined the clusters as the maxima of the density field smoothed on the scale $R \sim 1.5h^{-1} \text{ Mpc}$ and have defined their peculiar velocities using the same smoothing scale as for the density field. In this way, the sizes of all clusters are the same and do not depend on the richness of the cluster. Our study shows that in this case the rms peculiar velocities of clusters increase with cluster richness. In other words, the rms peculiar velocities of peaks increase with the height of the peaks. We found that this result is not very sensitive to the power spectrum of density fluctuations. We tested also two other models with different power spectra ($n = -1$ and a Λ CDM model) and found that the rms peculiar velocity increases with cluster richness similarly in all models studied.

Our result is consistent with the result found by Colberg et al. (1998) for superclusters. Richer clusters are clustered more strongly and, therefore, in superclusters the rms mass of clusters is larger than for isolated clusters. Colberg et al. (1998) studied the peculiar velocities of clusters and found that the rms velocities for clusters which are members of superclusters are about 20% to 30% larger than those for isolated clusters. Therefore, more massive clusters in superclusters move faster than less massive clusters outside superclusters.

To examine the rms peculiar velocities of clusters for different moments between $\sigma_8 = 0.7$ to $\sigma_8 = 1.0$, we started from the cluster velocities at the moment $\sigma_8 = 0.8$ and $\sigma_8 = 0.84$, in models (1) and (2), respectively, and used the linear scaling, $v_{cl} \sim \sigma_8$. We tested this scaling in the model (1), by comparing the cluster velocities in N-body simulations at the moments when $\sigma_8 = 0.5$ and $\sigma_8 = 0.8$. The results are presented in Figure 5b. For $\Omega_0 = 0.4$ and $\sigma_8 = 0.7$, we show the rms cluster peculiar velocities determined by using N-body simulations of clusters when $\sigma_8 = 0.5$ (dashed line) and $\sigma_8 = 0.8$ (solid line). We see that the differences for clusters with $d_{cl} < 80h^{-1} \text{ Mpc}$ are very small. The difference is somewhat larger for massive clusters with a mean separation $d_{cl} > 80h^{-1} \text{ Mpc}$ ($\sim 5\%$). Therefore, during the evolution between $\sigma_8 = 0.5$ and $\sigma_8 = 0.8$, cluster velocities evolve almost as expected by the linear approximation.

The observed rms peculiar velocity of galaxy clusters was investigated in several recent papers (e.g. Bahcall, Gramann & Cen 1994, Bahcall and Oh 1996, Borgani et al. 1997b, Watkins 1997). In this paper we use the results obtained by Watkins (1997). He developed a likelihood method for estimating the rms peculiar velocity of clusters from line-of-sight velocity measurements and their associated errors. This method was applied to two observed samples of cluster peculiar velocities: a sample known as the SCI sample (Giovanelli et al. 1997) and a subsample of the Mark III catalog (Willick et al. 1997). Watkins (1997) found the rms one-dimensional cluster peculiar velocity of $265_{-75}^{+106} \text{ km s}^{-1}$, which corresponds to the three-dimensional rms velocity of $459_{-130}^{+184} \text{ km s}^{-1}$.

Figure 4 shows the limits for $\sigma_8 \Omega_0^{0.6}$ in different models, assuming that the observed cluster sample studied by Watkins (1997) corresponds to the model clusters with a mean cluster separation $d_{cl} \sim 30h^{-1} \text{ Mpc}$ ($n_{cl} = 3.70 \times 10^{-5} h^3 \text{ Mpc}^{-3}$). In the model (1), the rms peculiar velocity of clusters with a separation $d_{cl} = 30h^{-1} \text{ Mpc}$ is $459_{-130}^{+184} \text{ km s}^{-1}$, when $\sigma_8 = (0.33_{-0.09}^{+0.13}) f^{-1}(\Omega_0)$. For $\Omega_0 = 0.3$ and $\Omega_0 = 0.4$, we obtain $\sigma_8 = 0.68_{-0.19}^{+0.27}$ and $\sigma_8 = 0.57_{-0.16}^{+0.22}$,

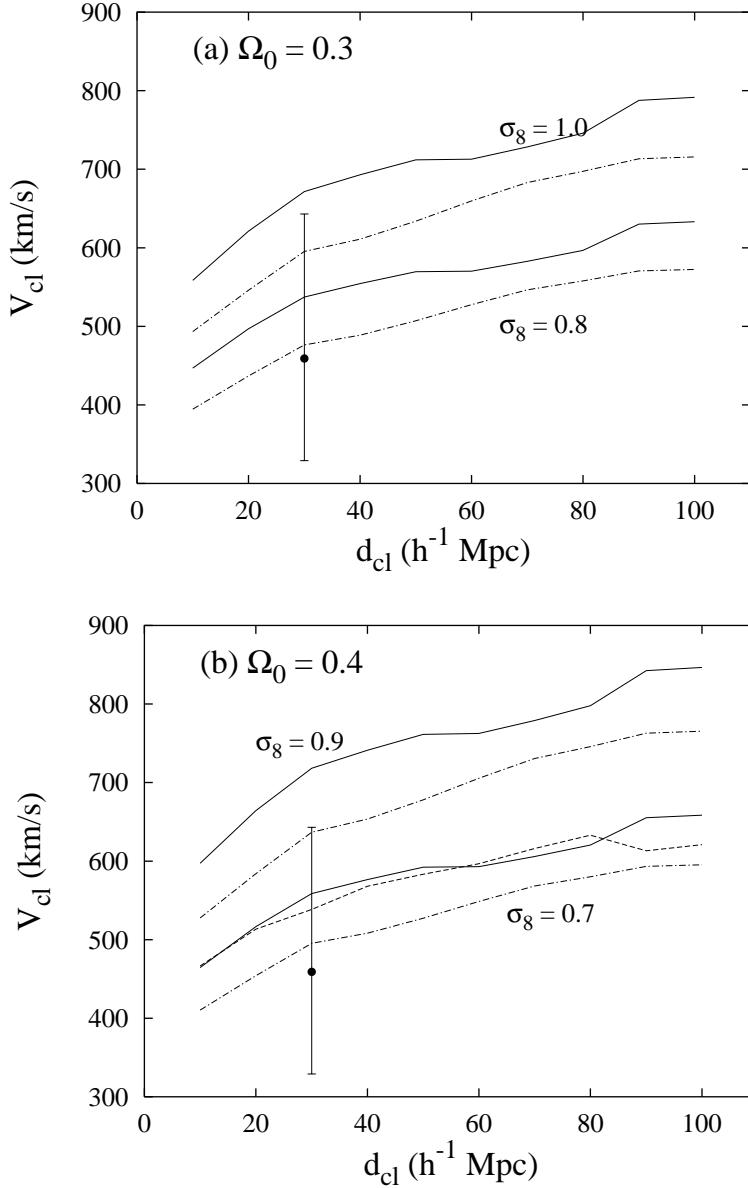


Figure 5. The rms peculiar velocities of clusters in the model (1) (solid lines) and in the model (2) (dot-dashed lines). The rms velocities are shown for different values of the mean cluster separation, d_{cl} . (a) The density parameter $\Omega_0 = 0.3$. The rms velocities are shown for $\sigma_8 = 0.8$ and for $\sigma_8 = 1.0$. (b) The density parameter $\Omega_0 = 0.4$. The rms velocities are shown for $\sigma_8 = 0.7$ and for $\sigma_8 = 0.9$. For $\sigma_8 = 0.7$, we show the rms cluster velocities determined by simulations when $\sigma_8 = 0.5$ (dashed line) and $\sigma_8 = 0.8$ (solid line). The filled circle shows the observed rms peculiar velocity of galaxy clusters.

respectively. For the power spectrum (2), we found that $\sigma_8 = (0.37^{+0.15}_{-0.10})f^{-1}(\Omega_0)$. Therefore, for $\Omega_0 = 0.3$ and $\Omega_0 = 0.4$, $\sigma_8 = 0.76^{+0.31}_{-0.21}$ and $\sigma_8 = 0.64^{+0.26}_{-0.17}$, respectively.

Now we can compare the observational constraints obtained by studying the mass function and peculiar velocities of clusters of galaxies. In the model (1) for $\Omega_0 = 0.4$, the mass function and the peculiar velocities of clusters are consistent with the observed data, for the small window of $\sigma_8 = 0.71 - 0.78$. For $\Omega_0 > 0.6$, the observed mass function and the peculiar velocities of clusters are not consistent with each other. Either the observed mass function of clus-

ters is overestimated or the peculiar velocities of clusters are underestimated. Therefore, in the model (1), the mass function and the peculiar velocities of clusters are consistent with observations only if $\Omega_0 < 0.6$. In the second model, the permitted window in the (Ω_0, σ_8) plane is larger. For $\Omega_0 = 0.4$, the mass function and the peculiar velocities are consistent with the observed data if $\sigma_8 = 0.72 - 0.88$. For example, for $\Omega = 0.4$ and $\sigma_8 = 0.75$, the number density of clusters with mass $M_{1.5} = 4 \times 10^{14} h^{-1} M_\odot$ is $n(> M) = 2.7 \times 10^{-6} h^3 \text{ Mpc}^{-3}$, and the rms peculiar velocity of clusters with a mean separation $d_{cl} = 30 h^{-1} \text{ Mpc}$ is 530 km s^{-1} .

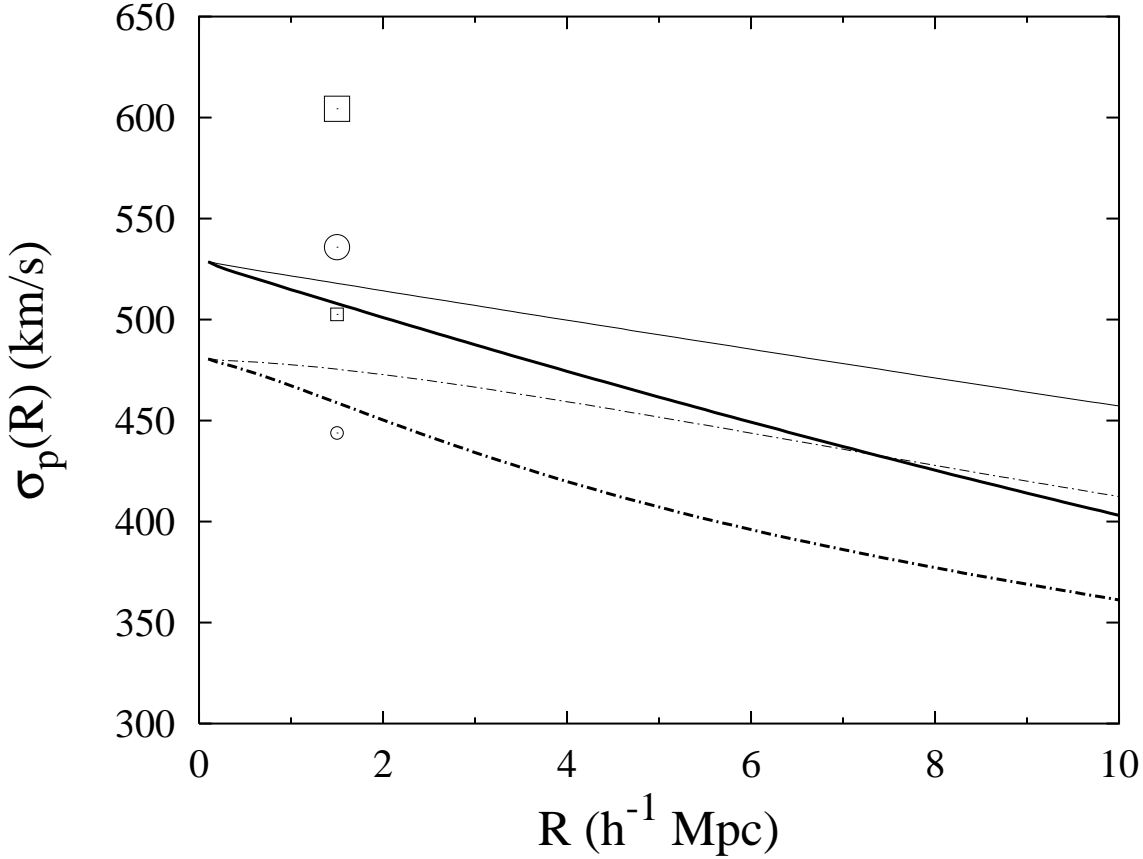


Figure 6. The rms peculiar velocity of peaks, $\sigma_p(R)$, for the power spectra (1) (heavy solid line) and (2) (heavy dot-dashed line) for $\Omega_0 = 0.3$ and $\sigma_8 = 0.9$. The light curves show the corresponding rms peculiar velocity $\sigma_v(R)$ for the same models. The small and large squares demonstrate the rms peculiar velocity of clusters in the model (1) with mean separations $d_{cl} = 10h^{-1}$ Mpc and $d_{cl} = 30h^{-1}$ Mpc, respectively. The small and large circles show the corresponding rms peculiar velocities in the model (2).

We investigated also the linear theory predictions for peculiar velocities of peaks in the Gaussian field. The linear rms velocity fluctuation on a given scale R can be expressed as

$$\sigma_v(R) = H_0 f(\Omega_0) \sigma_{-1}(R), \quad (8)$$

where σ_j is defined for any integer j by

$$\sigma_j^2 = \frac{1}{2\pi^2} \int P(k) W^2(kR) k^{2j+2} dk. \quad (9)$$

Bardeen et al. (1986) showed that the rms peculiar velocity at peaks of the smoothed density field differs systematically from $\sigma_v(R)$, and can be expressed as

$$\sigma_p(R) = \sigma_v(R) \sqrt{1 - \sigma_0^4 / \sigma_1^2 \sigma_{-1}^2}. \quad (10)$$

In this approximation, the rms velocities of the peaks do not depend on the height of the peaks.

Figure 6 shows the rms peculiar velocities of peaks, $\sigma_p(R)$, for the power spectra (1) and (2) for $\Omega_0 = 0.3$ and $\sigma_8 = 0.9$. We have used the top-hat window function. For comparison, we show also the rms peculiar velocity $\sigma_v(R)$ for the same models. For the cluster radius $R = 1.5h^{-1}$ Mpc, σ_p is lower than σ_v about $\sim 2\%$ and $\sim 3.5\%$ for models (1) and (2), respectively. On larger scales, the difference between

σ_p and σ_v increases. For comparison, we show in Figure 6 the rms peculiar velocity of clusters with mean separations $d_{cl} = 10h^{-1}$ Mpc and $d_{cl} = 30h^{-1}$ Mpc, derived by using N-body simulations. The rms peculiar velocity of clusters with a separation $d_{cl} = 10h^{-1}$ Mpc is similar to the linear theory expectations at the scale $R \sim 1.5h^{-1}$ Mpc. (It is slightly smaller ($\sim 2\%$) than σ_p at the radius $R = 1.5h^{-1}$ Mpc. This small difference is probably caused by smoothing inherent to particle-mesh method).

The peculiar velocity of rich clusters is higher than that predicted by the linear approximation (10). In the model (1), the peculiar velocity of clusters with a mean separation $d_{cl} = 30h^{-1}$ Mpc is $\sim 19.0\%$ higher than σ_p at the radius $R = 1.5h^{-1}$ Mpc. In the model (2), the peculiar velocity of these clusters is $\sim 16.8\%$ higher than that predicted by the linear theory. These results are in good agreement with the results obtained by Colberg et al. (1998). They compared the peculiar velocities of galaxy clusters with $\sigma_p(R)$ at larger radii, $R \sim 8h^{-1}$ Mpc, and for this reason found a larger difference ($\sim 40\%$) between the rms peculiar velocity of galaxy clusters and σ_p .

In Figure 5, we showed that during the evolution between $\sigma_8 = 0.5$ and $\sigma_8 = 0.8$, the rms peculiar velocities of clusters with a mean separation $d_{cl} < 80h^{-1}$ Mpc evolve

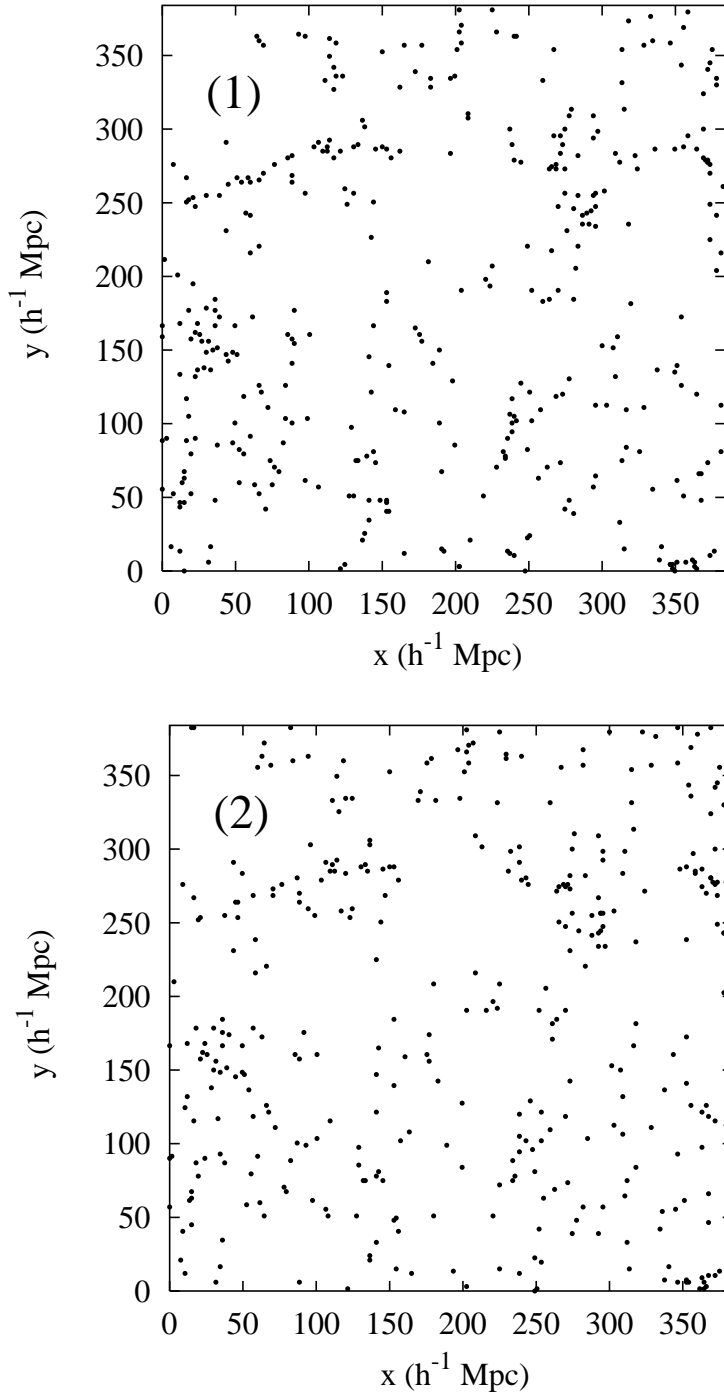


Figure 7. Panel (a) shows the distribution of clusters in a $96h^{-1}$ Mpc thick slice in the model (1). Panel (b) shows the distribution of clusters in the same slice in the model (2). The distribution is shown for the clusters with a mean separation $d_{cl} = 34h^{-1}$ Mpc.

as expected by the linear theory, $v_{cl} \sim \sigma_8$. The difference between the linear approximation (10) and the peculiar velocities of the $d_{cl} = 30h^{-1}$ Mpc clusters must therefore arise when $\sigma_8 < 0.5$. Further study is needed to investigate the nonlinear evolution of peculiar velocities of clusters in more detail.

4 THE POWER SPECTRUM OF CLUSTERS OF GALAXIES

Figure 7 shows the spatial distribution of clusters with a mean separation $d_{cl} = 34h^{-1}$ Mpc in our models. Figure 7a shows the distribution of clusters for the initial power spectra (1) and Figure 7b for the initial spectra with a primordial feature at wavelengths $\lambda \sim 30 - 60h^{-1}$ Mpc (equation [2]).

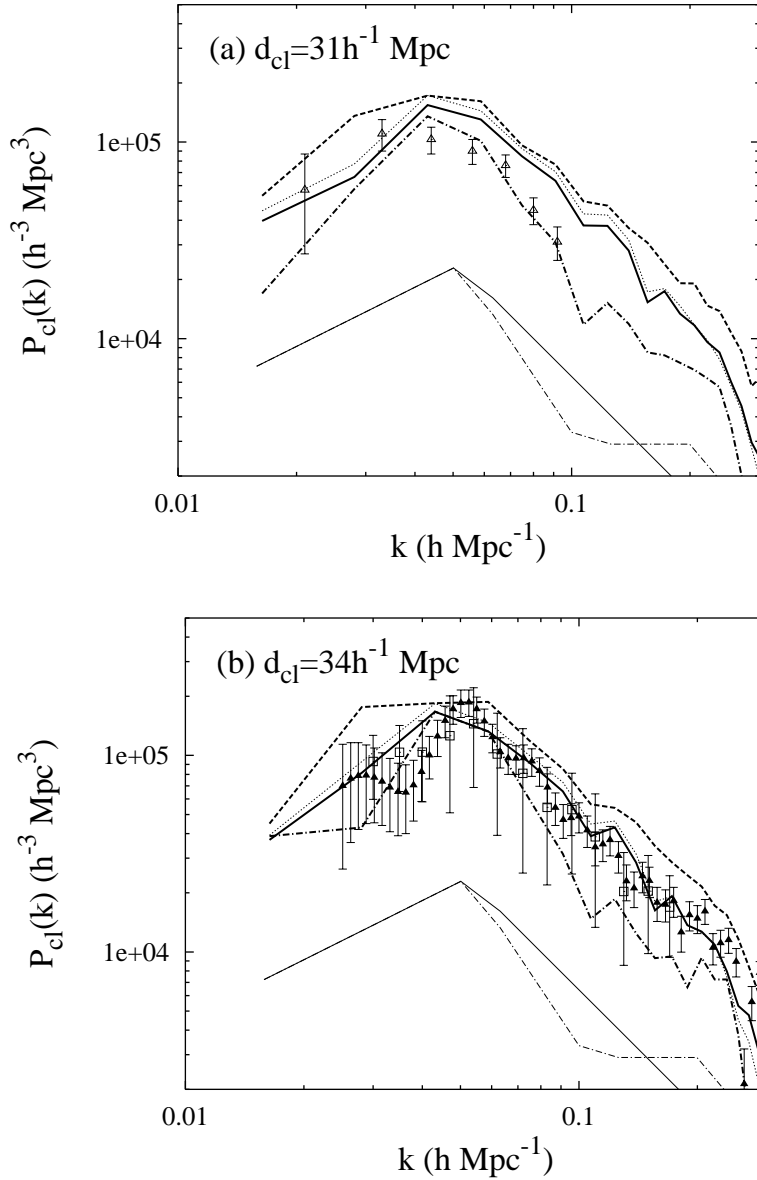


Figure 8. The redshift-space power spectrum of clusters in the model (1) for $\sigma_8 = 0.8$ (solid lines) and in the model (2) for $\sigma_8 = 0.84$ (dot-dashed lines). The heavy curves show the power spectra of clusters and the light curves the corresponding linear power spectra of matter fluctuations. To transform the clusters to the redshift space we have assumed that $\Omega_0 = 0.3$. The dotted line demonstrates the redshift-space power spectrum of clusters in the model (1) for $\Omega = 1$. The dashed line represents the power spectrum of clusters in the model (1) for $\sigma_8 = 0.5$. (a) The power spectrum of model clusters and APM clusters (open triangles) with a mean separation $d_{cl} = 31h^{-1}$ Mpc. (b) The power spectrum of model clusters and Abell clusters with a separation $d_{cl} = 34h^{-1}$ Mpc. Filled triangles and open squares show the power spectrum of Abell clusters as determined by Einasto et al. (1997a) and Retzlaff et al. (1998), respectively.

The phases of the initial density fluctuations were chosen to be the same, and therefore, we see directly the influence of the initial power spectrum. At a first look, the distribution of clusters in different models is rather similar. However, we see that the shape of superclusters in different models is slightly different. In the model (1), the clusters inside superclusters are more concentrated, while in the model (2), superclusters are larger and the clusters within superclusters

are more disperse (compare, e.g., the large superclusters in the upper-left corner). The bump in the initial power spectrum at $\lambda \sim 30 - 60h^{-1}$ Mpc influences the distribution of clusters inside superclusters.

Figure 8 demonstrates the redshift-space power spectrum of clusters, $P_{cl}(k)$. The clusters were determined in the simulation at the moment when $\sigma_8 = 0.8$ and $\sigma_8 = 0.84$, in the models (1) and (2), respectively. To calculate the power

spectrum we transformed the cluster positions to the redshift space, determined the density field on a 128^3 grid using the CIC scheme and calculated its Fourier components, subtracting the shot noise term.

To transform the clusters from the real space to the redshift space, we determined the peculiar velocities of clusters in the simulations with $\Omega = 1$ and used the linear scaling, $v_{cl} \sim f(\Omega_0)$, for $\Omega_0 = 0.3$. In this case the peculiar velocities of clusters are consistent with observations for $\sigma_8 \sim 0.8$ (see Figure 5). However, $P_{cl}(k)$ is not very sensitive to this assumption. In Figure 8 we show also the power spectrum of clusters in the redshift space for the model (1) for $\Omega = 1$, where the peculiar velocities of clusters are severely overestimated, $v_{cl} \sim 1100 \text{ km s}^{-1}$. In this model $P_{cl}(k)$ at wavenumbers $k < 0.1h^{-1} \text{ Mpc}$ is $\sim 10\%$ higher than for $\Omega_0 = 0.3$.

We investigated also the cluster power spectrum in the model (1) for $\sigma_8 = 0.5$ (here we used $\Omega = 1$). We found that during the evolution between $\sigma_8 = 0.5$ and $\sigma_8 = 0.8$, the power spectrum of clusters with a mean separation $d_{cl} \leq 30h^{-1} \text{ Mpc}$ is almost unchanged. For richer clusters, $P_{cl}(k)$ somewhat decreases ($\sim 14\%$ and $\sim 29\%$ for the clusters with $d_{cl} = 31h^{-1} \text{ Mpc}$ and $d_{cl} = 34h^{-1} \text{ Mpc}$, respectively.) This effect is probably caused by merging of very rich clusters. Further study (e.g. numerical simulations with higher dynamical range) is needed to determine whether this is a real effect for the model (1), or a numerical effect due to the limited dynamical range of the N-body simulations.

Let us compare the power spectra of clusters in our models with the observed power spectra of the APM and Abell clusters. Figure 8a shows the power spectrum of model clusters with a mean separation $d_{cl} = 31h^{-1} \text{ Mpc}$. For comparison, we show the power spectrum of the observed APM clusters determined by Tadros, Efstathiou & Dalton (1998). They analyzed the redshift survey of 364 clusters described by Dalton et al. (1994). The mean intercluster separation of the APM clusters is $d_{cl} \sim 31h^{-1} \text{ Mpc}$ (Dalton et al. 1994). Figure 8a shows that the power spectrum of the APM clusters is in good agreement with the power spectrum of clusters predicted in the model (2). In the model (1), the power spectrum of clusters is higher than observed (factor of ~ 1.8 at $k \sim 0.07 - 0.08h \text{ Mpc}^{-1}$).

Figure 8b demonstrates the power spectrum of model clusters and the Abell clusters with a mean separation $d_{cl} = 34h^{-1} \text{ Mpc}$. We show the power spectra of the Abell clusters determined by Einasto et al. (1997a) and Retzlaff et al. (1998). Einasto et al. (1997a) determined the power spectrum of the Abell clusters from the correlation function of clusters, while Retzlaff et al. (1998) estimated the power spectrum directly from the Fourier space. We see that the power spectra estimated by different methods are consistent with each other. However, the error bars measured by Retzlaff et al. (1998) are much larger than calculated by Einasto et al. (1997a) and probably underestimated in the latter case (see Retzlaff et al. 1998, Einasto et al. 1997a for details). Figure 8b shows that the power spectrum predicted in the model (1) for $\sigma_8 = 0.8$ is consistent with the observed power spectrum of the Abell clusters. For $\sigma_8 = 0.5$, the amplitude of density fluctuations at wavenumbers $k > 0.1h \text{ Mpc}^{-1}$ is higher than observed. The power spectrum of clusters in the model (2) is consistent with the observed power spectrum measured by Retzlaff et al. (1998) within the uncertainties.

We investigated also the relation between the power

spectrum of clusters and the power spectrum of matter fluctuations. During the evolution the power spectrum of clusters, $P_{cl}(k)$, is almost unchanged, while the power spectrum of matter fluctuations evolves as $P(k) \sim \sigma_8^2$ in the linear regime. In this case, the bias parameter $b_{cl}^2(k) = P_{cl}(k)/P(k) \sim \sigma_8^{-2}$ and therefore, in order to compare different models at different moments, it is reasonable to express the parameter b_{cl} in terms of σ_8 . We examined the bias parameter b_{cl} at the wavenumber interval $k \sim 0.06 - 0.08h \text{ Mpc}^{-1}$. In the model (1) for $\sigma_8 = 0.8$, we found that $b_{cl} = 2.30/\sigma_8$ and $b_{cl} = 2.40/\sigma_8$ for the clusters with $d_{cl} = 31h^{-1} \text{ Mpc}$ and $d_{cl} = 34h^{-1} \text{ Mpc}$, respectively. (For $\sigma_8 = 0.5$, as the cluster power spectrum is somewhat larger, the $b_{cl} = 2.45/\sigma_8$ and $b_{cl} = 2.70/\sigma_8$, respectively). In the model (2) for $\sigma = 0.84$, we obtain that $b_{cl} = 2.25/\sigma_8$ and $b_{cl} = 2.50/\sigma_8$, respectively. In this model, the bias parameter is similar to the model (1). The relation between the distribution of matter density and of clusters of different richness is studied in more detail in the paper by Gramann & Suhhonenko (1998).

5 THE CORRELATION FUNCTION OF CLUSTERS OF GALAXIES

In this Section we examine the spatial two-point correlation function of clusters, $\xi_{cl}(r)$, in our models. To determine the correlation function, we first transformed cluster positions to the redshift space and then determined the correlation function of clusters by pair counting.

Figure 9 shows the redshift-space correlation function of clusters in the model (1) for $\sigma_8 = 0.8$ and in the model (2) for $\sigma_8 = 0.84$. The peculiar velocities were calculated for the density parameter $\Omega_0 = 0.3$. We investigated also the $\Omega = 1$ model for velocities and found that in this case $\xi_{cl}(r)$ at radii $r = 10 - 20h^{-1} \text{ Mpc}$ is $\sim 16\%$ higher than for $\Omega_0 = 0.3$. Figure 9 shows also the correlation function in the model (1) for $\sigma_8 = 0.5$. During the evolution in the model (1), the correlation function of clusters, as the power spectrum of clusters, somewhat decreases ($\sim 22\%$ and $\sim 38\%$, at $r \sim 15h^{-1} \text{ Mpc}$, for the $d_{cl} = 31h^{-1} \text{ Mpc}$ and $d_{cl} = 34h^{-1} \text{ Mpc}$ clusters, respectively). This effect is probably caused by merging of rich clusters.

Now we can compare the correlation function of clusters predicted in the models with the observed correlation function of the APM and Abell clusters. Figure 9a demonstrates the correlation function of model clusters and of the APM clusters with a mean separation $d_{cl} = 31h^{-1} \text{ Mpc}$. The correlation function of the APM clusters has been determined by Dalton et al. (1994). On small scales the correlation function in the model (2) is in good agreement with the correlation function of the APM clusters. The correlation function of the APM clusters is equal to unity at a pair separation $r_0 = 14.3 \pm 1.75h^{-1} \text{ Mpc}$ (Dalton et al. 1994). In the model (2) we find that $r_0 = 14 \pm 1h^{-1} \text{ Mpc}$.

On larger scales, $\xi_{cl}(r)$ in the model (2) is larger than that measured by Dalton et al. (1994) for the APM clusters. On the other hand, the power spectrum of clusters on large spatial scales in the model (2) is in good agreement with the power spectrum of the APM clusters determined by Tadros, Efstathiou & Dalton (1998) (Figure 8a). This comparison suggests that the correlation function of clusters determined

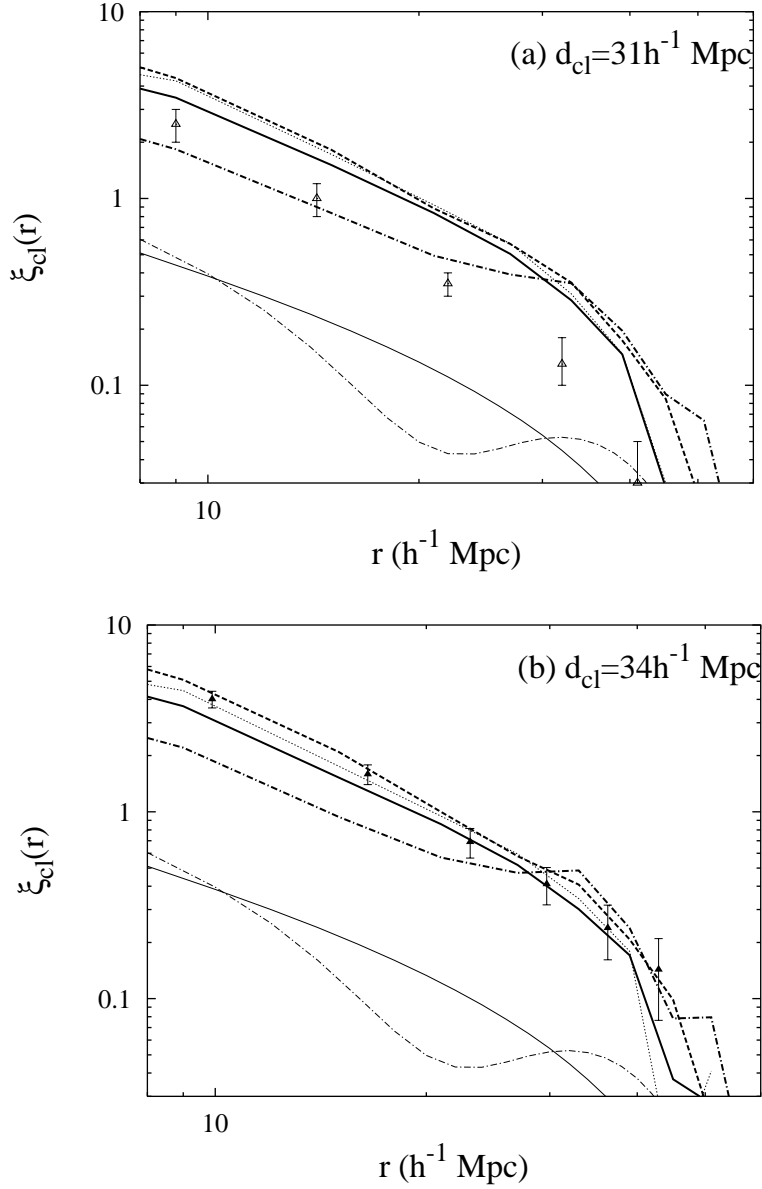


Figure 9. The redshift-space correlation function of clusters in the model (1) for $\sigma_8 = 0.8$ (solid lines) and in the model (2) for $\sigma_8 = 0.84$ (dot-dashed lines). The heavy curves show the correlation function of clusters and the light curves the corresponding linear correlation function of matter fluctuations. To transform the clusters to the redshift space we have assumed that $\Omega_0 = 0.3$. The dotted line demonstrates the redshift-space correlation function of clusters in the model (1) for $\Omega = 1$. The dashed line represents the correlation function of clusters in the model (1) for $\sigma_8 = 0.5$. (a) The correlation function of model clusters and APM clusters (open triangles) with a mean separation $d_{cl} = 31h^{-1}$ Mpc. (b) The correlation function of model clusters and Abell clusters (filled triangles) with a separation $d_{cl} = 34h^{-1}$ Mpc.

by Dalton et al. (1994) may be underestimated at large separations $r > 20h^{-1}$ Mpc. In the model (1), $\xi_{cl}(r)$ is higher than observed on all scales. In this model $r_0 = 19 \pm 1h^{-1}$ Mpc.

Figure 9b shows the spatial correlation function of clusters with a separation $d_{cl} = 34h^{-1}$ Mpc. For comparison, we present the correlation function of the Abell clusters determined by Einasto et al. (1997c). On small scales the cor-

relation function of the Abell clusters is higher than that observed for the APM clusters. We find that $r_0 = 20 \pm 3h^{-1}$ Mpc for the Abell clusters. This effect is partly due to differences in the number densities of the APM and Abell clusters. However, our models predict that the correlation function of clusters with a mean separation $d_{cl} = 31h^{-1}$ Mpc and $d_{cl} = 34h^{-1}$ Mpc is very similar. (In the models (1) and (2), the correlation length of clusters with $d_{cl} = 34h^{-1}$

Mpc is $r_0 = 20 \pm 1h^{-1}$ Mpc and $r_0 = 15 \pm 1h^{-1}$ Mpc, respectively.) The correlation function of the Abell clusters at separations $r < 25h^{-1}$ Mpc is probably overestimated due to the projection and selection biases known to affect clustering in the Abell cluster catalogues (e.g. Sutherland 1988). On larger separations these effects are not so important. The correlation function of clusters in the models (1) and (2) is consistent with the observed correlation function of the Abell clusters on separations $r > 25h^{-1}$ Mpc. We examined also the radius at which the cluster correlation function $\xi_{cl}(r_1) = 0$. We found that $r_1 = 54 \pm 3h^{-1}$ Mpc and $r_1 = 60 \pm 3h^{-1}$ Mpc, in the models (1) and (2), respectively. For the Abell clusters, the parameter $r_1 = 50 \pm 10h^{-1}$ Mpc.

Thus, the model (2) fits the correlation function of the APM clusters on small scales and the correlation function of Abell clusters on large scales. This model predicts that there is a bump in the correlation function of clusters at separations $r \sim 20 - 35h^{-1}$ Mpc. Available data are insufficient to confirm or to rule out this interesting possibility. Accurate measurements of the correlation function of clusters at these distances can serve as a discriminating test for this model.

6 CONCLUSIONS

In this paper, we have examined the properties of clusters of galaxies in two cosmological models. In the first model, the initial power spectrum was chosen in the form $P(k) \propto k^{-2}$ at the wavelengths $\lambda < 120h^{-1}$ Mpc (equation 1). In the second model, we assumed that the initial power spectrum contains a primordial feature at the wavelengths $\lambda \sim 30 - 60h^{-1}$ Mpc (equation 2). The density fluctuations at these wavelengths influence the distribution of clusters inside superclusters. In the model (2), superclusters are larger and the clusters inside superclusters are not so concentrated than in the model (1) (see Figure 7). We investigated the mass function, peculiar velocities, the power spectrum and the correlation function of clusters in both models for different values of Ω_0 and σ_8 . Below, we briefly summarize the results obtained.

(1) The mass function of clusters of galaxies in models (1) and (2), when compared at a same values of Ω_0 and σ_8 , is very similar for smaller masses $M \leq 4 \times 10^{14}h^{-1}M_\odot$. For larger masses the mass function in the model (2) is steeper than in the model (1). For $\Omega_0 = 0.3$ and $\Omega_0 = 0.4$, the mass function of clusters in both our models is consistent with observations, if $\sigma_8 = 0.90 \pm 0.12$ and $\sigma_8 = 0.80 \pm 0.09$, respectively.

(2) The rms peculiar velocities of clusters in the model (2) are $\sim 12\%$ smaller than in the model (1), when compared at the same values of Ω_0 and σ_8 . In the model (1), the rms peculiar velocity of clusters is consistent with observations if $\sigma_8 = (0.33_{-0.09}^{+0.13})\Omega_0^{-0.6}$. In this model, the mass function and the peculiar velocities of clusters are consistent with observations only if $\Omega_0 < 0.6$. For $\Omega_0 = 0.4$, the mass function and the peculiar velocities are consistent with the observed data if $\sigma_8 = 0.71 - 0.78$. In the model (2), the rms peculiar velocity of clusters is consistent with observations if $\sigma_8 = (0.37_{-0.10}^{+0.15})\Omega_0^{-0.6}$ and the permitted region in the (Ω_0, σ_8) plane is larger. For $\Omega_0 = 0.4$, the mass function and the peculiar velocities are consistent with the observed data if $\sigma_8 = 0.72 - 0.88$.

(3) The redshift-space power spectrum of clusters in the model (2) is in good agreement with the observed power spectrum of the APM clusters. The power spectrum of clusters in this model is also consistent with the observed power spectrum of the Abell clusters within uncertainties. In the model (1), the power spectrum of clusters is higher than observed for the APM clusters (factor of ~ 1.8 at $k \sim 0.07 - 0.08h$ Mpc $^{-1}$).

(4) The redshift-space correlation function of clusters in the model (2) is consistent with the correlation function of the APM clusters at small distances $r < 25h^{-1}$ Mpc. At larger separations the cluster correlation function in this model is consistent with the correlation function as derived for the Abell clusters. In the model (1), the correlation function of clusters on small distances is higher than observed for the APM clusters.

Therefore, in many aspects the power spectrum of density fluctuations in the model (2) fits the observed data better than the simple power law model (1). The superclusters of galaxies in the Universe are probably more disperse as predicted in the model (2) and not so concentrated as predicted in the model (1). Observed data are not sufficient to examine the power spectrum of density fluctuations at wavelengths $\lambda \sim 30 - 120h^{-1}$ Mpc in more detail, but our study suggests that probably at these wavelengths the initial power spectrum is not a featureless simple power law.

We examined also the linear theory predictions for peculiar velocities of peaks in a Gaussian field and compared these with the peculiar velocities of clusters in N-body simulations. We determined the clusters as the maxima of the density field smoothed on the scale $R \sim 1.5h^{-1}$ Mpc and defined their peculiar velocities using the same smoothing scale as for the density field. In this way, the sizes of all clusters are the same and do not depend on the richness of the cluster. Our study shows that in this case the rms peculiar velocities of clusters increase with cluster richness. The rms peculiar velocity of small clusters is similar to the linear theory expectations, while the rms peculiar velocity of rich clusters is higher than that predicted in the linear theory.

ACKNOWLEDGEMENTS

We thank E. Saar, J. Einasto and J. Colberg for useful discussions. This work has been supported by the ESF grant 97-2645.

REFERENCES

- Bahcall, N.A., Cen, R. 1993, ApJ, 407, L49 (BC93)
- Bahcall, N.A., Gramann, M., Cen, R. 1994, ApJ, 436, 23
- Bahcall, N.A., Oh, S.P. 1996, ApJ, 462, L49
- Bardeen, J.M., Bond, J.R., Kaiser, N., Szalay, A.S. 1986, ApJ, 304, 15
- Baugh, C., Efstathiou, G. 1993, MNRAS, 265, 145
- Borgani, S. et al. 1997a, NewA, 1, 321
- Borgani, S., Da Costa L.N., Freudling, W., Giovanelli, R., Haynes, M.P., Salzer, J., Wegner, G., 1997b, ApJ, 482, L121
- Broadhurst, T.J., Ellis, R.S., Koo, D.S., Szalay, A.S. 1990, Nature, 343, 726
- Bunn, E.F., White, M. 1997, ApJ, 480, 6
- Carlberg, R.G., Yee, H.K.C., Ellingson, E. 1997, ApJ, 479, L19

- Colberg, J.M., et al. 1998, MNRAS, submitted (astro-ph: 9805078)
- da Costa, L.N., Vogeley, M.S., Geller, M.J., Huchra, J.P., Park, C. 1994, ApJ, 437, L1
- Dalton, G.B., Croft, R.A.C., Efstathiou, G., Sutherland, W.J., Maddox, S.J., Davis, M. 1994, MNRAS, 271, L47
- Efstathiou, G., Frenk, C.S., White, S.D.M., Davis, M. 1988, MNRAS, 235, 715
- Einasto, J., et al. 1997a, Nature, 385, 139
- Einasto, J., et al. 1997c, MNRAS, 289, 801
- Einasto, M., Tago, E., Jaaniste, J., Einasto, J., Andernach, H. 1997b, A&AS, 123, 119
- Eisenstein, D.J., Hu, W., Silk, J., Szalay, A.S. 1998, ApJ, 494, L1
- Eke, V. R., Cole, S., Frenk, C. S. 1996, MNRAS, 282, 263
- Girardi, M., Borgani, S., Giuricin, G., Mardirossian, F., Mezetti, M. 1998, ApJ, 506, 45 (G98)
- Giovanelli, R. et al. 1997, AJ, 113, 22
- Gramann, M. 1988, MNRAS, 234, 569
- Gramann, M. 1993, ApJ, 405, L47
- Gramann, M. 1998, ApJ, 493, 28
- Gramann, M., Suhhonenko, I. 1998, ApJ, submitted
- Katgert, P., Mazure, A., den Hartog, R., Adami, C., Biviano, A., Perea, J., 1998, A & AS, 129, 399
- Lacey, C., Cole, S. 1994, MNRAS, 271, 676
- Lahav, O., Rees, M.J., Lilje, P.B., Primack, J.R. 1991, MNRAS, 251, 128
- Landy, S.D., Shectman, S.A., Lin, H., Kirshner, R.P., Oemler, A., Tucker, D., Schechter, P.L. 1996, ApJ, 456, L1
- Lesgourgues, J., Polarski, D., Starobinsky, A.A., 1998, MNRAS, 297, 769
- Navarro, J.F., Frenk, C.S., White, S.D.M. 1996, ApJ, 462, 563
- Nusser, A., Colberg, J.M. 1998, MNRAS, 294, 457
- Peacock, J.A. 1997, MNRAS, 284, 885
- Press, W.H., Schechter, P. 1974, ApJ, 187, 425
- Retzlaff, J., Borgani, S., Gottlöber, S., Müller, V. 1998, New Astron., in press (astro-ph: 9709044)
- Starobinsky, A.A., 1992, JETP Lett., 55, 477
- Sugiyama N. 1995, ApJS, 100, 281
- Sutherland, W.J. 1988, MNRAS, 234, 159
- Tadros, H., Efstathiou, G. 1996, MNRAS, 282, 1381
- Tadros, H., Efstathiou, G., Dalton, G. B. 1998, MNRAS, 296, 995
- Watkins, R. 1997, MNRAS, 292, L59
- Willick, J.A., Courteau S., Faber, S. M., Burstein, D., Dekel, A., Strauss, M. A., 1997, ApJS, 109, 333
- White, S. D. M., Efstathiou, G., & Frenk, C. S. 1993, MNRAS, 262, 1023